Available online at www.sciencedirect.com
SCIENCE DIRECT
Journal of Photochemistry and Photobiology A: Chemistry 176 (2005) 39–49
Journal of Photochemistry and Photobiology A:Chemistry
www.elsevier.com/locate/jphotochem

Measurement and modelling of UV radiation penetration and photolysis rates of nitrate and hydrogen peroxide in Antarctic sea ice: An estimate of the production rate of hydroxyl radicals in first-year sea ice

M.D. King [a,*], J.L. France [a], F.N. Fisher [b], H.J. Beine [c]

[a] *Department of Geology, Royal Holloway University of London, Egham, Surrey TW20 0EX, UK*
[b] *Department of Chemistry, Kings College London, Strand, London WC2R 2LS, UK*
[c] *C.N.R IIA, Institute for Atmospheric Pollution, Via Salaria Km 29,3, CP10, Monterotondo Scalo I-00016, Roma, Italy*

Available online 23 September 2005

Abstract

Sea ice may be an oxidising medium owing to sunlight-driven reactions occurring within the ice. UV light transmission and albedo (320–450 nm) are reported for first-year sea ice in Terra Nova Bay, Antarctica, in conjunction with depth integrated photolysis rates for OH radical production from photolysis of hydrogen peroxide (H_2O_2) and nitrate anion (NO_3^-). The albedo is 0.70–0.75 and the transmission is characterised by an *e*-folding depth of ∼50 cm or an extinction coefficient of $\sim 2\,m^{-1}$. A coupled atmosphere-snowpack radiation-transfer model (TUV-snow) was applied to the experimental measurements so that scattering and absorption cross-sections of the ice could be deduced. These cross-sections were used to model actinic flux (spherical irradiance) profiles in the ice, and thus illustrate the enhancement of actinic flux around a depth of 10 cm in the sea ice for zenith angles smaller than 50°. The actinic flux-depth profiles demonstrate how extinction coefficients (measured at solar zenith angles greater than 50°) for the top 10–20 cm of sea ice are much larger than extinction coefficients measured deeper in the ice. The TUV model was also used to calculate photolysis frequencies for nitrate anions and hydrogen peroxide, which produce hydroxyl radicals within the sea ice. The depth integrated photolysis rate of hydrogen peroxide is an order of magnitude larger than the depth integrated photolysis rate of nitrate. However, the low concentrations of hydrogen peroxide in sea water and ice relative to nitrate result in a higher rate of production of OH radicals for nitrate than hydrogen peroxide. Approximate upper limits for depth integrated rate of production OH from nitrate photolysis in a 1 m deep sea ice block were found to be 0.06–2 $\mu mol\,m^{-2}\,h^{-1}$ for solar zenith angles of 85–45°, respectively. The depth integrated production rate of OH radical from hydrogen peroxide photolysis is 0.01–0.3 $\mu mol\,m^{-2}\,h^{-1}$ for solar zenith angles of 85–45°, respectively. Photolysis of nitrate in ice is an efficient route to the production of hydroxyl radicals and an oxidising ice. It must be stressed that these depth integrated rates of production are, however, approximate upper limits because the low porosity and the microphysical, chemical and photochemical process occurring in sea ice may reduce the depth integrated rate of production. In conclusion we suggest that first-year sea ice may be an efficient medium for photochemistry and that 85% of ice photochemistry may occur in the top 1 m of sea ice, assuming that the concentration of chromophore (nitrate or hydrogen peroxide) and photochemical efficiency are independent of depth in the sea ice.

Keywords: Ice; Sea ice; Snow; Nitrate; Hydrogen peroxide; OH; Irradiance; Actinic flux; Antarctica

1. Introduction

Sea ice can cover a total area of $34.5 \times 10^6\,km^2$ at its maximum extent, 7% of the surface of the Earth [1]. The freezing of sea water changes the albedo of the sea surface and provides a habitat for many marine species [2]. The study of the optical properties of sea ice has traditionally been considered to be important for three reasons. First, sea ice is important for biological production. Sea ice algae flourish in new and aging sea ice and grow in and underneath first-year sea ice. This accounts for 25% of primary production in ice covered Antarctic waters. The irradiance is the limiting variable for several biological processes including: the growth of algae [3], the uptake of dissolved nitrogen [4] and microbial growth [5]. The annual production of carbon due to biological processes in the Antarctic sea ice is 40 Tg [6]. There is evidence of a biological feedback mechanism that may limit sea ice extent, with phytoplankton biomass altering the absorption properties of sea ice and increased solar

* Corresponding author. Tel.: 44 1784 413586.
E-mail address: m.king@gl.rhul.ac.uk (M.D. King).

1010-6030/$ – see front matter © 2005 Elsevier B.V. All rights reserved.
doi:10.1016/j.jphotochem.2005.08.032

absorption of the sea ice resulting in a 6% decrease in ice cover in the winter [7]. Secondly, the heat budget of the sea ice and partitioning of incident solar radiation between ocean, atmosphere and ice is critical to the summer melt-cycle of sea ice [8]. Perovich reported that during the SHEBA experiment 24% of incident radiation on the sea ice was absorbed by the snow and ice [8]. The ice optical properties (especially scattering) are important to the ice–atmosphere system energy budget [9]. Thirdly, in climatic studies it is important to understand the amount of radiation absorbed by ice for the sea ice climate feedback mechanism to be quantified [10,11]. Recent work has highlighted that the absorption properties of impurities (e.g. anthropogenic soot) within the ice may lead to strengthening of the feedback mechanism [12,13].

Recently the optical properties of snow have been studied with reference to photochemistry in or on snow and ice [14]. Experiments in polar regions have shown that photochemistry in snow and ice can have a major effect on the biogeochemistry of the atmosphere and snowpacks. There have been many measurements of gaseous fluxes of nitrogen oxides from sunlit snowpacks [15–24]. Laboratory work has demonstrated that the source of NO_x in snow is the photolysis of the nitrate anion [25–31]:

$$NO_3^- + h\upsilon \rightarrow NO_2^- + O, \quad (1)$$

$$NO_3^- + h\upsilon \rightarrow NO_2 + O^-. \quad (2)$$

The results of photochemical modelling of the snowpacks have demonstrated that the fluxes of NO_x from the snowpack are consistent with a photolytic source [20,32–35].

The oxygen radical anion produced in reaction (2) may react with the water to generate the reactive OH radical:

$$O^- + H_2O \rightarrow OH + OH^-, \quad (3)$$

thus making the snowpack an oxidising medium. It has recently been shown that OH radical can be formed from the photolysis of hydrogen peroxide in ice [36]:

$$H_2O_2 + h\upsilon \rightarrow OH + OH. \quad (4)$$

Photochemical pathways involving the OH radical in snowpacks are implicated in the production of fluxes of acetaldehyde and formaldehyde that have been observed from snowpacks [26,37–45,46]. Many other organic compounds including alkyl nitrates, alkenes, halides and organic acids may have a snowpack photolytic source [26,38,47–51]. Recent work has also demonstrated that organic pollutants contained within snow and ice in polar regions may photolyse [52,53]. It is suggested that photochemical reactions of nitrate and hydrogen peroxide may also be occurring in sea ice. In sea ice, one could speculate that the OH radical may react with the brine to liberate gaseous halogen species that may be responsible for the polar ozone depletions in Arctic regions [54].

In this work we record the optical properties of a first-year sea ice and model the radiation-transfer within that sea ice to calculate the first-order rate constant for the production of OH radicals from nitrate and hydrogen peroxide photolysis. We believe this is the first time that the abiotic photochemistry of sea ice has been considered quantitatively.

As several good reviews of the optics of sea ice exist [8,55,56], only a brief summary will be given here. The optical properties of sea ice are governed by the weak absorption of water, absorptions by impurities in the ice, the scattering owing to the microstructure of the ice and the asymmetry factor, g, of the sea ice. The microstructure of sea ice is described in detail elsewhere [57,58]. Briefly, the sea ice is a mixture of ice platelets, brine pockets, precipitated salts and air bubbles, the proportions of which depend on temperature [8]. Light is scattered at the interfaces of these microstructures, and thus sea ice is a highly scattering medium for photons. Although the scattering by air bubbles is greater than by brine pockets [8], typically there are more brine pockets (24 mm^{-3}) than air bubbles (1 mm^{-3}) [57]. There have been several studies of the beam spread function [59–62] and shape of the radiance field within the ice [63,64]. The light field within the sea ice at depth is asymptotic, not fully isotropic, and decays exponentially. The deviation from spherical symmetry is small and may be due to the ice forming aligned platelets separated by brine [63]. The decay of the diffuse radiation in the sea ice can be described by the Bouger–Beer–Lambert law,

$$I(z) = I(z')e^{-k(\lambda)(z'-z)} \quad (I)$$

where $I(z)$ is the irradiance at depth z, $I(z')$ the irradiance at an another depth z' and $k(\lambda)$ is the extinction coefficient. In work on the optical properties of snow [35,65,66] it has been common to describe the characteristic length of light penetration into the snow using the asymptotic e-folding depth, $\varepsilon(\lambda)$,

$$\varepsilon(\lambda) = \frac{1}{k(\lambda)} \quad (II)$$

The asymptotic e-folding depth, $\varepsilon(\lambda)$, is the depth at which incident diffuse irradiance has been reduced to $1/e$ (∼37%) of its initial value. The e-folding depth in snowpack is often reported as liquid equivalent e-folding depth, $\varepsilon_{liq}(\lambda)$, which is equal to the product of the asymptotic e-folding depth and the ratio of the density of the snow to that of liquid water. The scattering of photons within the ice is strongly forward peaked with the asymmetry factor taking values of 0.95 [67] or 0.975–0.995 [64]. Several spectral radiation-transfer models exist for modelling light fluxes in ice [8,55,56,59,60,64,68–71], but, to the authors' knowledge, none have been used to calculate photolysis rate constants in ice.

The aim of this work was to record the optical properties (albedo and e-folding depth) of first-year sea ice at Terra Nova Bay, to model these data with an adapted radiative-transfer model for a coupled atmosphere-snow system, and to predict the depth profile of spherical actinic irradiance and the photolysis rate constant for nitrate photolysis within the sea ice. This work is exploratory; the experiments and subsequent modelling described here arose from the chance to study the sea ice during a time when bad weather prevented the study of the photochemistry of snowpacks as part of the CESIP campaign.

In the work presented in this paper, the term 'actinic flux' refers to 'spherical irradiances', i.e. the number of photons

passing through the surface of a sphere (for photolysis calculations), and 'irradiance' will be used to describe the flux of photons through a plane (the instrumental measurement).

2. Experimental

2.1. Location

Measurements were conducted on the sea ice in Terra Nova Bay, Antarctica (74°40.594′S, 164°07.813′E), on the 25th November 2004. The location was the focus of a campaign to monitor the biological activity under the sea ice. The area studied consisted of a bare section of sea ice approximately 50 m in diameter. Although aerial photographs (taken from a helicopter and on the kilometre scale) of the local area revealed that the sea ice was approximately 40% covered in windblown snow (approximately 10–20 cm deep on a 10 m scale) the area of sea ice chosen for study was not covered by more than a few mm of snow. The site was approximately 200 m away from the extent of the sea ice station and the nearest fissure or crack in the sea ice was approximately 100 m away. The skylight conditions during all the measurements were diffuse with thick low cloud. The sea ice temperatures were −5 to −9 °C. Depth resolved sea ice temperature measurements were not possible. Three days after the measurements were taken the sea ice broke up.

2.2. Transmission measurements

A narrow (<5 cm) auger was used to drill holes into the sea ice. Material from the sea ice was collected and handled with clean plastic gloves. A stainless-steel irradiance probe was inserted vertically, facing downwards, into the hole and the hole was filled in with the sea ice material. At depths greater than 10 cm, a sea water–ice slush would assist filling the hole naturally. Irradiance measurements within the ice were recorded in the wavelength range 242–455 nm using a portable USB 2000 miniature fibre optic spectrometer from Ocean Optics. Light was guided into the spectrometer via a 4 m, 200 μm multi-mode fibre-optic fitted with a PTFE cosine corrector that also acted as a horizon for the fibre once the probe was inserted in the ice. One end of the fibre-optic was glued into a length of 0.64 cm diameter stainless steel tubing for protection and to act as a probe into the ice. The spectrometer was connected to a laptop computer running a LABVIEW programme, which recorded the spectra. The whole system ran on batteries. A second portable spectrometer (a Microtops II sunphotometer) was mounted vertically on a tripod and used to record the radiance of the downwelling atmospheric radiation and atmospheric column optical depth above the sea ice at 440 nm (10 nm FWHM). As stated previously, the atmospheric irradiance was diffuse with the thick low cloud. The Microtops II spectrometer covered the wavelength range 440–1020 nm in five separate 10 nm (FWHM) narrow Gaussian shaped bands.

Spectra of in-ice irradiance were recorded four to six times at each depth studied using different spectrometer integration times (0.1–59 s) to ensure an adequate signal was recorded even at the shorter wavelengths (≤350 nm). The probe was then removed from the ice and the hole drilled 5–10 cm deeper. This process was repeated further down through the ice pack until the signal-to-noise ratio became detrimental or the extent of the sea ice was reached, typically 1–1.5 m depth. Three holes were investigated in the sea ice with each hole taking ∼30 min to study, data from only one hole is presented. Measurements of the sky downwelling irradiance were made simultaneously with the in-ice measurements using the Microtops II spectrometer. Several of these downwelling sky radiance measurements were recorded for each spectrum recorded in the sea ice and averaged so that changes in the incident solar radiation on the sea ice could be observed for the whole of the integration period of the ice spectrometer. Each irradiance measurement in the ice was thus corrected for very small external fluctuations such as cloud cover by dividing the sea ice irradiance measurement by the atmospheric downwelling irradiance. Measurements were taken during stable sky conditions and when the sun was close to its zenith, i.e. around local noon.

The wavelength calibration of the ice probe spectrometer was performed in the field using the mercury lines of a portable fibre-coupled Hg–Ar lamp. Dark spectra were recorded in the field by placing a thick, light-proof cap over the end of the probe. Spectra were recorded using each of the integration times used in the intensity measurements. Intensity calibrations for the ice probe spectrometer were performed after the fieldwork at room temperature and pressure using a NIST-traceable tungsten filament lamp (Ocean Optics). Laboratory studies showed that reducing the ambient temperature of the spectrometer from +15 to −15 °C decreased the number of counts recorded in dark spectra but did not affect the number of counts recorded from the NIST-traceable calibration light source.

The ice irradiance data were summed into 1 nm bins, corrected for dark current, hot pixels and standard lamp calibrations from both spectrometers. The ice spectra were then corrected by the Microtops II irradiance values. For each 1 nm bin, the value of the irradiance was plotted versus depth and an exponential fit was undertaken to yield the asymptotic *e*-folding depth. The procedure is one we developed to study the radiative properties of snow in the Cairngorm Mountains [35].

2.3. Albedo measurements

Albedo measurements of the ice surface were undertaken using a GER1500 spectrometer. The reflectance of the surface was recorded, followed by the reflectance of a standard spectralon plate under the same skylight conditions so that the reflectivity of the bare sea ice relative to that of the reflectance standard could be determined. The albedo spectra were recorded above the ice at heights of about 1, 100 and 1000 m giving circular target areas of 0.05, 5 and 50 m in diameter, respectively. Measurements at the latter two heights, 100 and 1000 m, were conducted from a helicopter and the operator supported the instrument manually, thus it is likely that the diameters of the target areas are larger than the quoted 5 and 50 m, respectively. The albedo data for all three altitudes agree to within 10%. The

albedo data were recorded from the helicopter to increase the footprint of the albedo, and thus average over any small (<1 cm) surface heterogeneity.

2.4. Modelling

The radiative-transfer in atmosphere and the sea ice was modelled using the TUV atmosphere-snow coupled model [32], allowing the prediction of irradiances (flat plate and spherical) and photolysis rates. We believe this is the first time the model has been applied to sea ice. The model uses an empirical approach to obtain two variables that describe the optical properties of the ice (snow): the scattering coefficient, r_{scatt}, and the absorption coefficient for impurities, μ^+. The coefficients r_{scatt} and μ^+ are related to the coefficients σ_{scatt} and σ^+_{abs} by the density, ρ, of the sea ice:

$$\sigma_{\text{scatt}} = \frac{r_{\text{scatt}}}{\rho}, \tag{III}$$

$$\sigma^+_{\text{abs}} = \frac{\mu^+}{\rho}. \tag{IV}$$

The albedo or the *e*-folding depth of the sea ice can be reproduced in the model using many different pairs of values for μ^+ and r_{scatt}. However, only one set of values μ^+ and r_{scatt} will describe both the albedo and the *e*-folding depth of the sea ice. The techniques used to derive μ^+ and r_{scatt} are explained in detail elsewhere [32] and only a brief summary will be given here. The TUV model is used to calculate *e*-folding depths and albedos for different values of r_{scatt} and μ^+. A range of values of r_{scatt} and μ^+ are determined to reproduce either the measured *e*-folding depth or albedo over the wavelength range 350–449 nm. A plot of r_{scatt} versus μ^+ has two curves (one for *e*-folding depth and one for albedo). The values of r_{scatt} and μ^+ representing $\varepsilon(\lambda)$ and $a(\theta,\lambda)$ for the sea ice is represented by the intersection of these two curves. In practise, a small locus of intersections exists, one for each wavelength.

After the optical properties (μ^+ and r_{scatt}) of the sea ice are determined, the model can be used to predict the depth profile of actinic flux at various solar zenith angles. The photolysis rates of nitrate, $J(NO_3^-)$, and hydrogen peroxide $J(H_2O_2)$ within the ice were calculated for different solar zenith angles. The nitrate absorption cross-section of Burley and Johnson [72] with an extrapolation to 360 nm was used. The quantum yields for nitrate photolysis were taken from Dubowski et al. [29] The quantum yield values of Chu and Anastasio [25] could also be used and the *J* rates, depth integrated photolysis rates (transfer velocities) or depth integrated production rates presented later can be modified by multiplying by the ratio of the two measurements of quantum yields, as the quantum yields are wavelength independent in this region of the spectrum [25,29]. The absorption cross-section and quantum yield data for hydrogen peroxide was taken from the work of Chu and Anastasio [36]. The model was run for a 1 m thick ice sheet. An asymmetry factor, *g*, of 0.95 [67], 80 atmospheric levels each of 1 km and 30 ice levels were used. The albedo of the under-ice sea water was taken to be 0.08 and wavelength independent.

Depth integrated photolysis rates (transfer velocity, T_v) in the sea ice for nitrate and hydrogen peroxide photolysis were calculated:

$$T_v(NO_3^-) = \int_{z=0}^{z=1} J(NO_3^-)\,dz, \tag{V}$$

$$T_v(H_2O_2) = \int_{z=0}^{z=1} J(H_2O_2)\,dz. \tag{VI}$$

The product of the depth integrated photolysis rate (transfer velocity) and the concentration of nitrate or hydrogen peroxide is equal to the depth integrated production rate of hydroxyl radicals:

$$\text{Depth integrated production rate} = T_v(NO_3^-) \times [NO_3^-] \tag{VII}$$

$$\text{Depth integrated production rate} = T_v(H_2O_2) \times [H_2O_2] \tag{VIII}$$

Note in previous studies of photolysis of nitrate in the snowpack the depth integrated production rate was equal to the flux of photoproduct released from the snowpack to the atmosphere. The photoproducts in sea ice are not expected to leave the ice matrix.

3. Results

Fig. 1 shows that the light intensity decreased exponentially with depth in the sea ice, demonstrating that the attenuation of UV–vis diffuse radiation in ice is consistent with the Beer–Lambert law. The line fitted to the data in Fig. 1 was

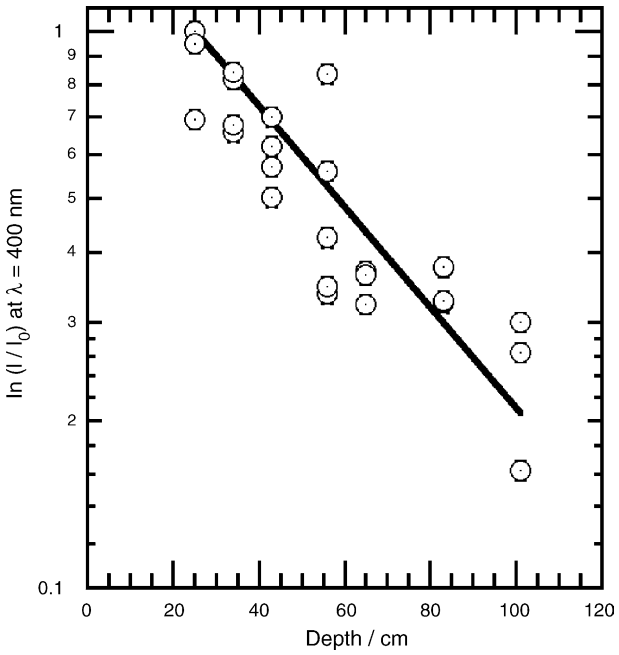

Fig. 1. Plot of $\ln\left[\frac{I(z)}{I(z')}\right]$ against ice depth, *z*, for $\lambda = 400$ nm. $I(z)$ is the light intensity at depth *z* in the sea ice and $I(z')$is the light intensity at the depth of the first measurement, i.e. 20 cm.

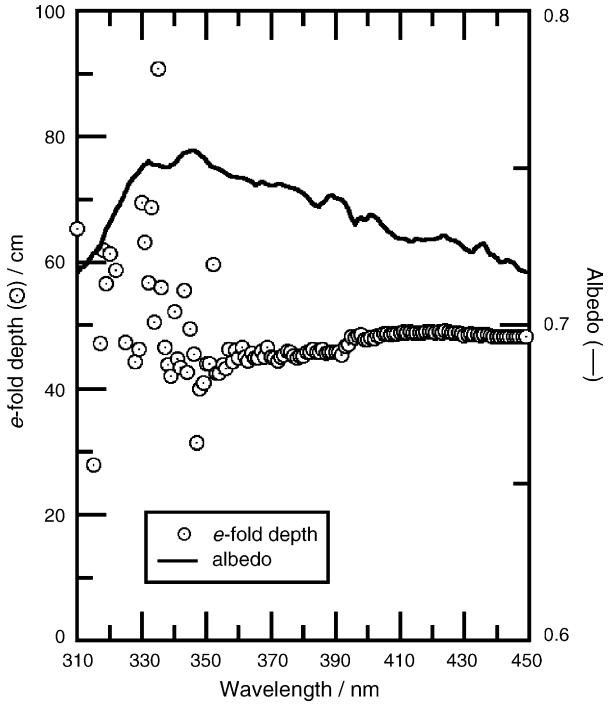

Fig. 2. Albedo and *e*-folding depths vs. wavelength for Antarctic sea ice.

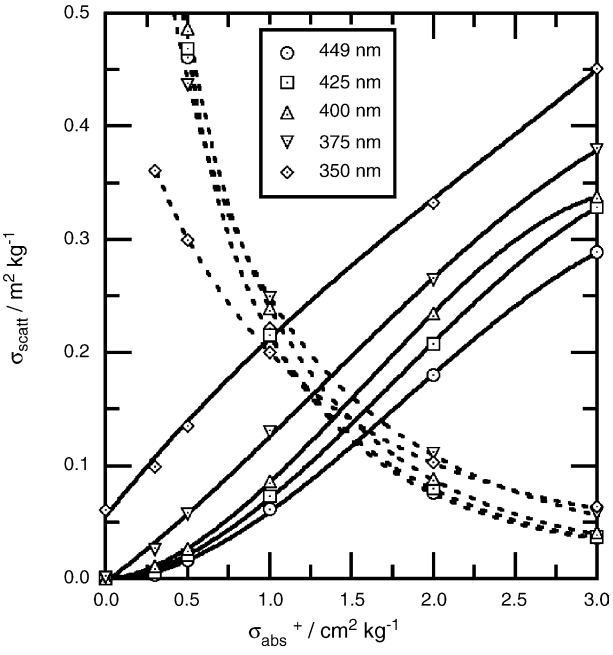

Fig. 3. A plot of modelled curves of σ_{scatt} vs. σ_{abs}^{+} for constant albedo and constant *e*-folding depth at five wavelengths, 350, 375, 400, 425 and 449 nm. The curves increasing from left to right (solid lines) represent constant surface albedo and those decreasing from left to right (dashed lines) represent constant *e*-folding depth. The intersection of these curves represents the values of σ_{scatt} and σ_{abs}^{+} used to describe the optical properties of the sea ice in this study.

calculated by a least squares fit of the data to Eq. (I), i.e. data were fitted in exponential form to determine ε, the *e*-folding depth. For the data fitted in Fig. 1, the *e*-folding depth is 48.0 cm. Eq. (I) is used to fit the depth resolved intensity data for each wavelength studied and determine the *e*-folding depth. The resulting *e*-folding depths are plotted versus wavelength in Fig. 2. Fig. 2 demonstrates that the *e*-folding depths calculated from plots such as Fig. 1 are relatively independent of wavelength over the range of 340–450 nm. The scatter in the data corresponding to measurement made at wavelengths shorter than 340 nm is due to the very low light levels measured at these wavelengths. The average albedo of sea ice, taken from 100 and 1000 m, is also shown in Fig. 2. The *e*-folding depth for the wavelength range 300–450 nm is approximately 50 cm. Fig. 3 is a plot of modelled curves of σ_{scatt} and σ_{abs}^{+} for constant albedo and *e*-folding depth for the wavelengths 350, 375, 400, 425 and 449 nm. The curves increasing from left to right represent constant surface albedo and those decreasing from left to right represent constant *e*-folding depth. The intersection of these curves represents the values of σ_{scatt} and σ_{abs}^{+} used to describe the optical properties of the sea ice in this study. An example of a plot of modelled actinic flux at 450 nm with depth for several zenith angles is given in Fig. 4. The modelled photolysis rate of NO_3^- and H_2O_2 to produce OH radicals versus depth in a 1 m thick slab of sea ice are plotted in Figs. 5 and 6. It is immediately obvious that the photolysis of H_2O_2, molecule for molecule, is more efficient than the photolysis of nitrate for all zenith angles. The photolysis of H_2O_2 produces a factor of between 14 and 21 more OH than photolysis of nitrate (molecule for molecule), the low ratio corresponding to low solar zenith angles and deep in the sea ice and the higher values of the ratio corresponding to high solar zenith angles near the surface of the sea ice. These ratios are higher than the values predicted by Chu and Anastasio for snow [36]. Integrating $J(H_2O_2)$ and $J(NO_3^-)$ over depth gives the depth integrated photolysis rate of OH production (also known as transfer velocity). The depth integrated photolysis rates for OH production from photolysis of nitrate and hydrogen perox-

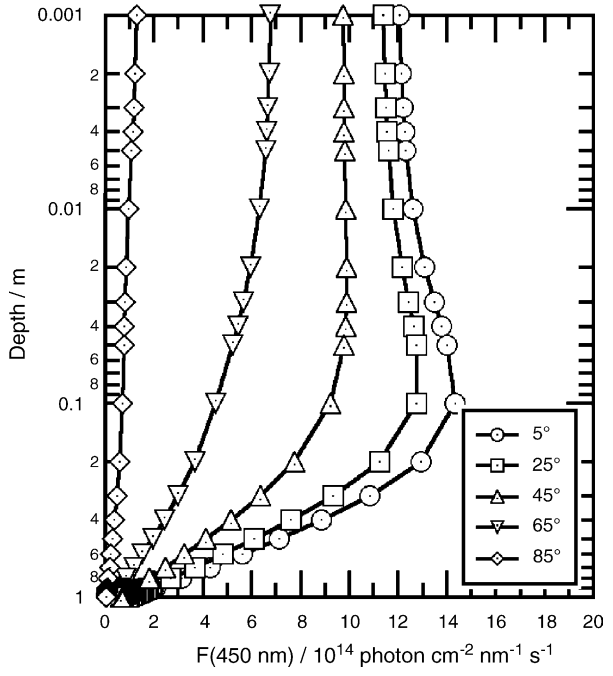

Fig. 4. A plot of the modelled actinic flux, $F(450\,nm)$ with depth in a 1 m ice sheet for several solar zenith angles.

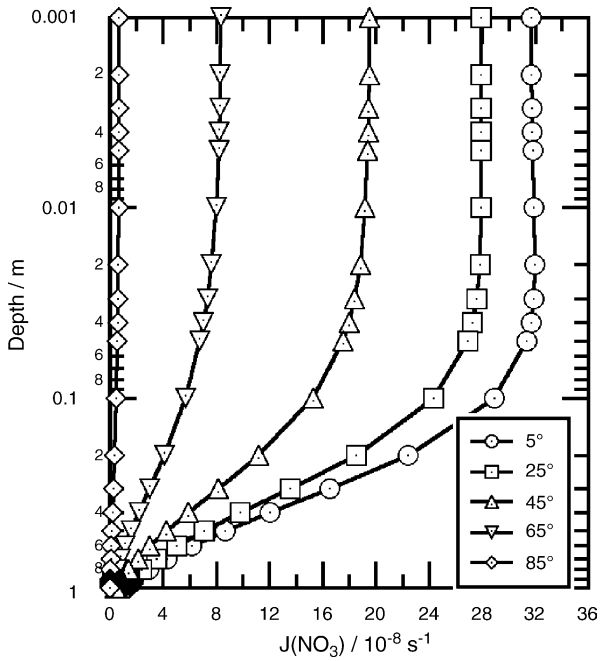

Fig. 5. A plot of $J(NO_3^-)$ vs. ice depth for several solar zenith angles.

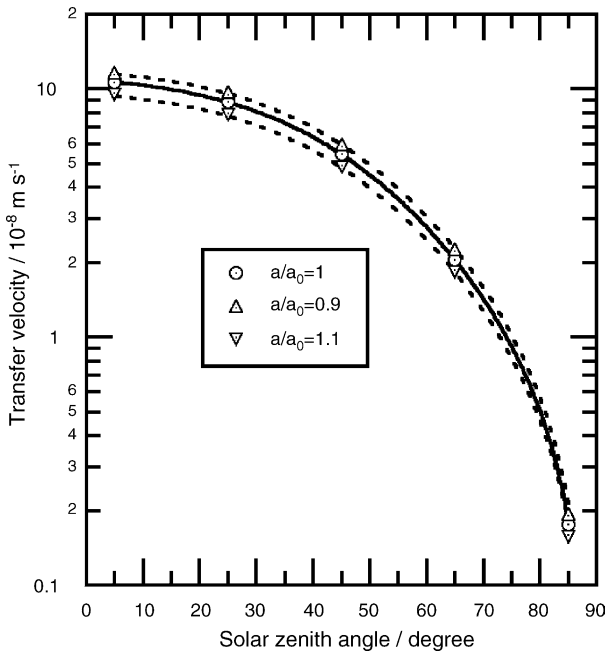

Fig. 7. Depth integrated photolysis rate (transfer velocity) for OH production from the photolysis of NO_3^- vs. zenith angle. The dashed lines represent the effect on the transfer velocity of increasing or decreasing the albedo by 10% in determining the optical properties (σ_{scatt} and σ_{abs}^{+}) of the ice, see Table 1. Multiplication of depth integrated photolysis rate by the concentration of nitrate in sea ice will give the depth integrated production rate of hydroxyl radicals.

ide are shown in Figs. 7 and 8. Also plotted in Figs. 7 and 8 are the depth integrated photolysis rates if the albedo of the sea ice were changed by 10%, i.e. varied within experimental uncertainty. Figs. 5–8 can be used to predict production rates and photolysis rates of OH radicals within sea ice for cloud free conditions anywhere on the planet simply from knowledge of the solar zenith angle and the concentrations of nitrate and hydrogen peroxide in sea ice. Volume production rate of hydroxyl radical at different depths can be calculated from Figs. 5 and 6 by multiplying the photolysis frequency, J, by the concentration

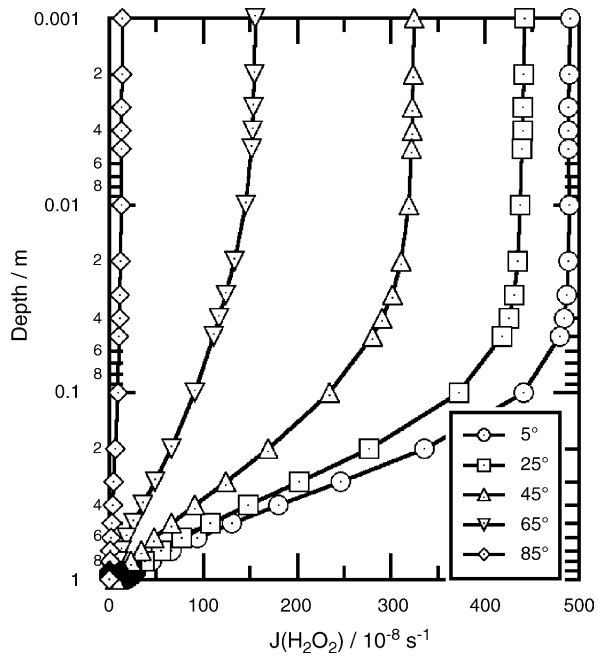

Fig. 6. Plot of $J(H_2O_2)$ vs. ice depth for several solar zenith angles.

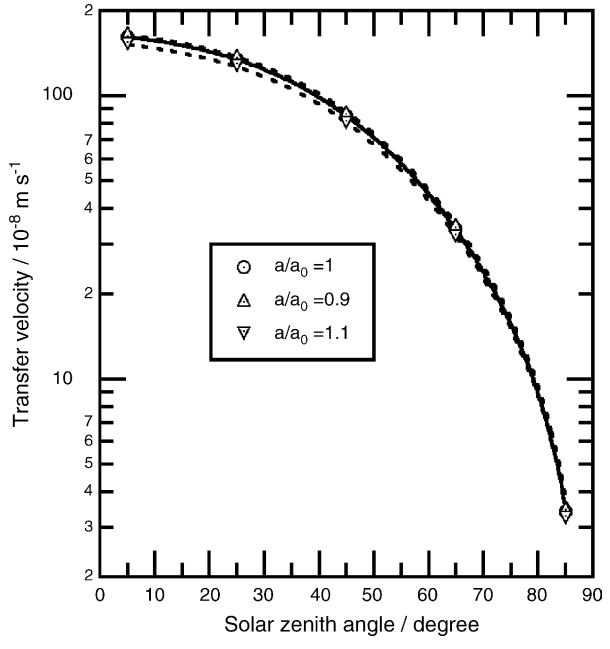

Fig. 8. Depth integrated photolysis rate (transfer velocity) for OH production from the photolysis of H_2O_2 vs. zenith angle. The dashed lines represent the effect on the depth integrated photolysis rate (transfer velocity) of increasing or decreasing the albedo by 10% in determining the optical properties (σ_{scatt} and σ_{abs}^{+}) of the ice, see Table 1. Multiplication of depth integrated photolysis rate by the concentration of hydrogen peroxide in sea ice will give the depth integrated production rate of hydroxyl radicals.

of nitrate or hydrogen peroxide. The depth integrated production rate of OH radicals can be calculated by multiplying the depth integrated photolysis rate (transfer velocity) from Figs. 7 and 8 by the concentration of nitrate or hydrogen peroxide. The zenith angles used to produce Figs. 3–6 are the same as those used in a previous study when photolysis in snowpack was considered [32] so that comparisons can readily be made, between sea ice and snow.

4. Discussion

The discussion presented here will focus on the following topics:

(1) Errors and model sensitivity.
(2) Comparison with other measurements of the albedo and penetration of UV–vis radiation in sea ice.
(3) Depth profiles of irradiance and rates of nitrate and hydrogen peroxide photolysis in ice, the oxidative capacity of the ice and OH production.

The errors in the determination of the scattering and absorption cross-sections depend on the experimental measurements of the *e*-folding depth and the albedo. The error in the *e*-folding depth arises from imprecision in the depth of the probe (estimated to be 1 cm) and the errors in the repeatability of the spectral measurements. The error in the depth is negligible compared with the error in repeatability. The relative error in the repeatability of the spectral measurements for this study was investigated by taking multiple spectra at a given depth and integration time in the same hole in the ice. The error and was found to be 9–14% but clustered around 10%. The albedo values were calculated using the GER1500 spectrometer and associated software from the NERC Field Spectroscopy Facility to compare the reflectance of the ice to that of a spectralon panel mounted on a tripod. Reliable measurements are achieved by repeated measurement of the reflectance of the sea ice followed by the panel, minimising the time between measurements. For the measurements made from the helicopter, the error is typically 9% as the helicopter had to land to record each reference spectrum of the spectralon plate. The ground-based measurements of the albedo have errors of ∼5–10%. The data modelled for the determination of the scattering and absorption coefficients is sensitive to the measured albedo, a, *e*-folding depth, ε, and density, ρ, of the sea ice. Table 1 contains the results of a sensitivity study where the values of a, ε and ρ, are increased and decreased by 10% to observe the effect on the modelled absorption and scattering cross-sections. As can be seen the cross-sections are most sensitive to the albedo data and fairly insensitive to the value of the *e*-folding depth and sea ice density—something also found when studying the optical properties of snowpack [35]. The errors in the albedo were propagated through to the determined transfer velocity, as shown in Figs. 7 and 8.

There have been many measurements made of sea ice albedo and these have been reviewed by Perovich [8,55,56] The albedo reported here is higher than that normally reported for first-year sea ice and this may be due to the draining of the brine from the top 10–15 cm of the ice and the light coating of snow (<2 mm) on some areas of the sea ice. Very few measurements of the transmission or penetration of UV–blue light into sea ice have been reported [63,73–77]. Fig. 9 is a plot of extinction coefficient, $k(\lambda)$ (reciprocal of the *e*-folding depth) versus wavelength, λ, for the penetration of UV and blue light into sea ice that has been reported by various groups and includes our data from Fig. 2. As can be seen from Fig. 9, our data are consistent with the first-year ice measurement of Perovich [75] and bounded by the extrapolated measurements [55] of Grenfell and Maykut [78] for white ice and melting blue ice. The *e*-folding depth measurement versus wavelength in this study appear to have a weaker dependence on wavelength than the few previous studies. The wavelength dependence of the *e*-folding depth is in part determined by the low concentration absorbing impurities within the ice, and thus it is not prudent to compare ice samples from different polar regions and habitats and expect agreement. Fig. 9 also demonstrates the superior wavelength resolution of our studies compared with previous band studies.

Table 1
Scattering, σ_{scatt}, and absorption, σ^{+}_{abs}, cross-sections determined for values of albedo, a, *e*-folding depth, ε, and density, ρ, for sea ice around 400 nm (first row of data)

a/a_0	$\varepsilon/\varepsilon_0$	ρ/ρ_0	σ_{scatt} ($m^2\ kg^{-1}$)	σ^{+}_{abs} ($cm^2\ kg^{-1}$)
1	1	1	0.15	1.45
0.9	1	1	0.095	1.9
1.1	1	1	0.23	1.02
1	0.9	1	0.18	1.65
1	1.1	1	0.12	1.0
1	1	0.9	0.15	1.4
1	1	1.1	0.16	1.5

A sensitivity analysis is also included where the albedo, *e*-folding depths and density are varied by 10% from a base case (a_0, ε_0 and ρ_0). The modelling was undertaken for a location of 74.11°S and 164°E on the 4th November 2004 with 300 DU of ozone column and the asymmetry factor, g, equal to 0.95.

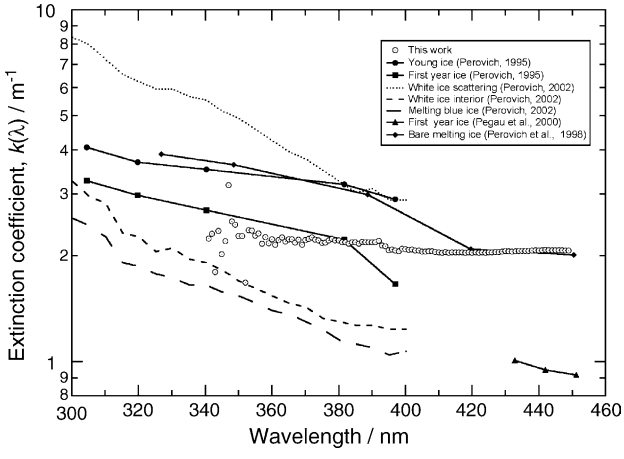

Fig. 9. A comparison of the extinction coefficients $k(\lambda)$ for the first-year sea ice studied in this work (open symbols) and other work in the region 300–460 nm. The data points represented by filled symbols are experimental measurements made by Perovich et al. [55,75] and Pegau et al. [63]. The dotted and dashed lines represent modelled extrapolations [55] of the original measurements by Grenfell and Maykut [78].

The depth profiles of sea ice actinic flux shown in Fig. 4 demonstrate that the sea ice (like clouds and snow) can be split into two zones based on the behaviour of the actinic flux with depth. Below ~20 cm in the sea ice the actinic flux, $F(\lambda)$, decays exponentially with depth and is essentially diffuse radiation. This model finding is supported by the experimental data, as shown in Fig. 1. In the top near-surface region of the sea ice, the direct radiation falling on the sea ice depends on the zenith angle. Photons in sea ice tend to be forward scattered (asymmetry factor, g, close to +1) and undergo a small angular change on each scattering event. A photon entering the sea ice has a higher probability of leaving the sea ice when at a glancing angle (high solar zenith angle) than at a large angle to the surface (low solar zenith angle) because the photon needs to be scattered through a smaller angle to leave the ice. At high solar zenith angles, >50°, the strong forward scattering behaviour of the sea ice leads to radiation escaping the sea ice and results in short e-folding depths (large extinction coefficients) near the surface. At low solar zenith angles, <50°, the light is propagated deeper into the sea ice, the direct radiation is converted to diffuse radiation and leads to an increase in the actinic flux around 10 cm, as shown in Fig. 4. The decrease in e-folding depth in the surface region of the sea ice at high solar zenith angles can be seen clearly by re-plotting the data in Fig. 4 as Fig. 10. Fig. 10 is a plot of the logarithm of actinic flux versus depth. The gradient of the lines in Fig. 10 are equal to the extinction coefficient (Eqs. (I) and (II)). In the near surface region, for zenith angles >50°, the gradients of the lines are larger than in the asymptotic region equating to larger extinction coefficients and smaller e-folding depths; there is a strong solar zenith angle dependency. In the asymptotic region the slopes of the lines (extinction coefficients) are independent of the solar zenith angles. It is in the asymptotic region that experimental e-folding depths are measured.

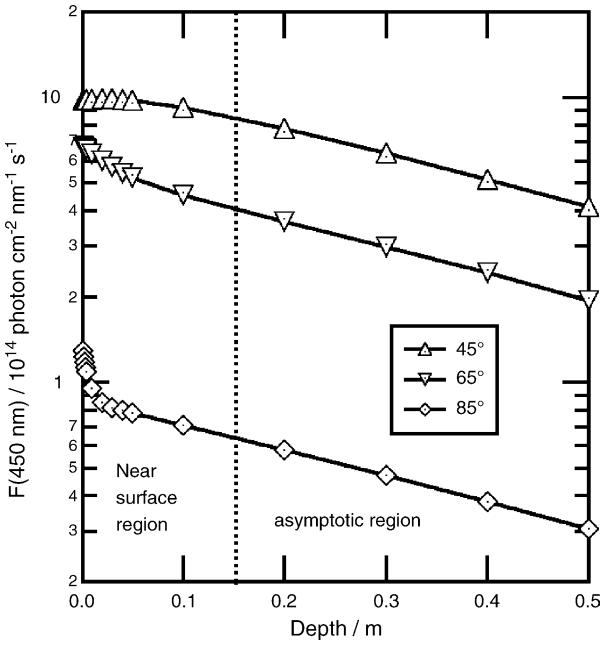

Fig. 10. A plot of modelled actinic flux at a wavelength of 450 nm vs. depth in sea ice. Three solar angles, 45°, 65° and 85° are considered. The graph is split into the near surface region where the radiation is a combination of direct and diffuse and an asymptotic region where the radiation is effectively all diffuse. The slope of the lines in the graph is equal to the extinction coefficient (see Eqs. (I) and (II)). For solar zenith angles greater than 50°, the extinction constant in the near surface region is clearly larger than in the asymptotic region. The extinction coefficient is independent of solar zenith angle in the asymptotic region. Thus, the e-folding depth (the reciprocal of the extinction coefficient) is smaller in the near surface region than in the asymptotic region, for solar zenith angles less than 50°.

The penetration and enhancement of actinic flux in sea ice is analogous to the situation in snow, which is explained in great detail elsewhere [32,34,66]. Sea ice, like snow, is an efficient medium in which to do photochemistry. The enhancements in actinic flux for a highly scattering low-absorption medium are shown in Simpson et al. [34]. The enhancement of actinic flux relative to downwelling actinic flux is due to conversion of direct radiation to diffuse radiation and the high albedo of the ice, which almost doubles the diffuse actinic flux near the surface of the sea ice [34]. The behaviour of actinic flux in the near surface region can be seen in the measurements of Perovich et al. [76]. These workers noted that in first-year, blue and green Arctic ice samples the extinction coefficient in the top layer of the sea ice was larger than in samples 20 cm lower in the sea ice, e.g. extinction coefficients of 5.6 m^{-1} in surface samples compared to 0.6 m^{-1} at lower depths. This is exactly the behaviour expected for large solar zenith angles. Caution should be exercised when comparing the spherical irradiances in Fig. 10 with the flat plate irradiances measured by Perovich et al. [76]. The enhancement of radiation near the surface of sea ice has been reported by another radiative-transfer modelling study [70]. These authors also demonstrated that cloud cover will reduce the enhancement of actinic flux as the cloud reduces the amount of direct radiation incident upon the ice surface. It should be noted that work presented in this paper does not discuss the alteration of the sea ice properties owing to biological absorbers in the ice. This is a topic for future work.

In previous work [65], it was reported that 85% of photochemistry in snowpack would occur within two e-folding depths of the surface of the snow (multiplying by e^{-2} will reduce a quantity to ~15% of its initial value). For cold, dry, polar (tundra) snow 85% of photochemistry occurs in the top 10 cm of snow [65], and for warm, wetter, mid-latitude (maritime) snow 85% of photochemistry occurs in the top 15–60 cm [35]. For the first-year sea ice studied here, 85% of photochemistry occurs in the top 1 m of sea ice. This measure assumes that the concentration and photochemical efficiency of the chromophore in the sea ice and snow are independent of depth.

It is non-trivial to convert the depth integrated photolysis rates into depth integrated production rates of OH radical from the sea ice (as shown by Eqs. (VII)–(VIII)) because the concentration of nitrate in the sea ice is not uniform, but heterogeneous. In abiotic ice, nitrate is a conservative molecule and is typically proportional to the salinity of the ice [79]. As the sea ice becomes colder, the nitrate will tend to be found in brine pockets as the ice desalinates [79]. The concentration of nitrate in sea ice measured in the field is reported to be depleted with respect to that expected by the measured salinity, owing to biological processes [79]. However, assuming the photochemistry to be the limiting

factor, the concentration of nitrate within the ice to be a uniform 10 μmol dm^{-3} [80], and using Eq. (VII), the depth integrated rates of production of OH radical are 0.06–2 μmol m^{-2} h^{-1} for solar zenith angles 85–45°, respectively. The calculations use data from Table 1 and Fig. 7 for a 1 m deep sea ice slab. It must be stressed that these are approximate upper limits because the low porosity and microphysical, chemical and photochemical processes occurring in sea ice may reduce the depth integrated rate of production. The depth integrated rate of production for the OH radical has been calculated—this does not imply a flux of OH molecules from the sea ice to the atmosphere. To the authors' knowledge there are no recent measurements of H_2O_2 in sea ice, however work on snow suggests the H_2O_2 is incorporated into the matrix of the ice [81]. Thus, to estimate a depth integrated production of OH radicals from photolysis of H_2O_2 in sea ice we assume a concentration of H_2O_2 in polar sea water to be 0.1 μmol dm^{-3} [82] and using Eq. (VIII) the depth integrated rates of production of OH radicals are 0.01–0.3 μmol m^{-2} h^{-1} for solar zenith angles 85–45°, respectively. There is great uncertainty in this value, as a reliable value for the concentration of H_2O_2 in sea ice could not be found. Hydrogen peroxide concentrations in snowpack have been reported two orders of magnitude higher as tabulated by Chu and Anastasio [36].

The penetration and enhancement of actinic flux in the sea ice can photolyse nitrate and hydrogen peroxide to produce OH radicals. In the presence of oxygen the sea ice will be an oxidising environment with the chemistry initiated by photo-produced hydroxyl radicals. Thomas and Papadimitriou [79] discuss the oxygen concentrations in sea ice and whether sea ice could become anoxic and clearly make the case that more work needs to be done. However, they counter speculation of anoxic sea ice by reviewing the measurements of abiotic sea ice that demonstrate that oxygen in brine pockets is supersaturated and depleted in the ice [79]. Thomas and Papadimitriou [79] also note that biology in the sea ice can reduce carbon dioxide concentration and raise oxygen concentrations. These observations are for sea ice systems that are closed and are not exchanging with the sea and atmosphere, yet remain oxic. In the study described in this work, the ice was porous to the sea water, and thus cannot be considered an oxygen poor environment. It therefore suggested that sea ice may be an oxidising medium.

5. Conclusions

Several conclusions may be drawn from this work:

1) Sea ice is an efficient medium for photochemical reactions. For solar zenith angles less than 50° there is an enhancement of actinic flux within the top 10 cm of the ice. Eighty-five percent of photochemistry will occur in the top 1 m of a sea ice column, assuming that the concentration of chromophore (nitrate or hydrogen peroxide) and photochemical efficiency are independent of depth in the sea ice.
2) The actinic flux-depth profiles demonstrates that sea ice (like snowpacks) can be split optically into two layers, a near surface layer and an asymptotic layer. The consideration of the direct and diffuse radiation in the near surface layer explains the previously experimentally measured *e*-folding depths measured near the surface of sea ice.
3) Nitrate photolysis rate constants, to produce OH radical in the top 10 cm of sea ice, are 3.2×10^{-7}, 2.8×10^{-7}, 2.0×10^{-7}, 0.8×10^{-7} and 0.07×10^{-7} s^{-1} for the solar zenith angles of 5°, 25°, 45°, 65° and 85°, respectively. Assuming a uniform concentration of nitrate in the sea ice of 10 μmol dm^{-3} allows an estimate of the upper limit of the depth integrated rate of production OH production of 0.06–2 μmol m^{-2} h^{-1} for solar zenith angles 85–45°, respectively.
4) Hydrogen peroxide photolysis rate constants, to produce OH radical in the top 10 cm of sea ice, are 4.8×10^{-6}, 4.3×10^{-6}, 3.1×10^{-6}, 1.4×10^{-6} and 0.13×10^{-6} s^{-1} for the solar zenith angles of 5°, 25°, 45°, 65° and 85°, respectively. Assuming a uniform concentration of hydrogen peroxide in the sea ice of 0.1 μmol dm^{-3} allows an estimate of the upper limit of the depth integrated rate of production OH production of 0.01–0.3 μmol m^{-2} h^{-1} for solar zenith angles of 85–45°, respectively.
5) The TUV-snow model can be used to model coupled sea ice-atmosphere systems as well as snow-atmosphere systems. The model can easily be adapted to study atmosphere-snow-ice systems found in the polar oceans.

Acknowledgements

M.D.K. wishes to thank NERC FSF for the loan and calibration of the GER1500 spectrometer (grant no. 447.0504), support from the Royal Society (54006.G503/24054/SM), Florent Domine for help with the airborne photography, Programma Nazionale di Ricerche in Antartide (PNRA (Italian Antarctic research program), Project no. 2004/6.2 BEINEX4 for financial and logistical support. F.N.F. wishes to thank King's College London for financial support. J.L.F. wishes to thank NERC for financial support (NER/S/A/200412177).

And lastly M.D.K. wishes to thank Professor Richard Wayne (mentor and friend) for teaching him research methods in photochemistry and how to be a scientist. This paper is dedicated to him and hopefully answers the question "What's all this about photochemistry in snow and ice?"

References

[1] G.S. Dieckmann, H.H. Hellmer, The importance of sea ice: an overview, in: D.N. Thomas, G.S. Dieckmann (Eds.), Sea Ice: An Introduction to its Physics, Chemistry, Biology and Geology, Blackwell Publishing, Oxford, 2005, pp. 1–21.
[2] K.R. Arrigo, D.N. Thomas, Antarctic Sci. 16 (4) (2004) 471–486.
[3] Y. Suzuki, S. Kudoh, M. Takahashi, J. Mar. Syst. 11 (1–2) (1997) 111–121.
[4] J.C. Priscu, M.P. Lizotte, G.F. Cota, A.C. Palmisano, C.W. Sullivan, Mar. Ecol.—Prog. Ser. 70 (2) (1991) 201–210.
[5] C.S. Cockell, P. Rettberg, G. Horneck, D.D. Wynn-Williams, K. Scherer, A. Gugg-Helminger, J. Photochem. Photobiol. B Biol. 68 (1) (2002) 23–32.
[6] K.R. Arrigo, D.L. Worthen, L.M.P.P. Dixon, G.S. Dieckmann, Science 276 (5311) (1997) 394–397.

[7] M. Manizza, C. Le Quere, A.J. Watson, E.T. Buitenhuis, Geophys. Res. Lett. 32 (5) (2005), art. no.-L05603.
[8] D.K. Perovich, Phys. B Condens. Matter 338 (1–4) (2003) 107–114.
[9] Z.H. Jin, K. Stamnes, W.F. Weeks, S.C. Tsay, J. Geophys. Res.-Oceans 99 (C12) (1994) 25281–25294.
[10] J.A. Curry, J.L. Schramm, E.E. Ebert, J. Climate 8 (2) (1995) 240–247.
[11] A. Hall, J. Climate 17 (7) (2004) 1550–1568.
[12] J. Hansen, L. Nazarenko, Proc. Natl. Acad. Sci. U.S.A. 101 (2) (2004) 423–428.
[13] S.G. Warren, Ann. Glaciol. 5 (1984) 177–179.
[14] F. Domine, P.B. Shepson, Science 297 (5586) (2002) 1506–1510.
[15] A.E. Jones, R. Weller, P.S. Anderson, H.W. Jacobi, E.W. Wolff, O. Schrems, H. Miller, Geophys. Res. Lett. 28 (8) (2001) 1499–1502.
[16] R.E. Honrath, M.C. Peterson, S. Guo, J.E. Dibb, P.B. Shepson, B. Campbell, Geophys. Res. Lett. 26 (6) (1999) 695–698.
[17] R.E. Honrath, M.C. Peterson, M.P. Dziobak, J.E. Dibb, M.A. Arsenault, S.A. Green, Geophys. Res. Lett. 27 (15) (2000) 2237–2240.
[18] R.E. Honrath, Y. Lu, M.C. Peterson, J.E. Dibb, M.A. Arsenault, N.J. Cullen, K. Steffen, Atmos. Environ. 36 (15–16) (2002) 2629–2640.
[19] H.J. Beine, F. Domine, A. Ianniello, M. Nardino, I. Allegrini, K. Teinila, R. Hillamo, Atmos. Chem. Phys. 3 (2003) 335–346.
[20] H.J. Beine, F. Domine, W. Simpson, R.E. Honrath, R. Sparapani, X.L. Zhou, M. King, Atmos. Environ. 36 (15–16) (2002) 2707–2719.
[21] A.E. Jones, R. Weller, E.W. Wolff, H.W. Jacobi, Geophys. Res. Lett. 27 (3) (2000) 345–348.
[22] X.L. Zhou, H.J. Beine, R.E. Honrath, J.D. Fuentes, W. Simpson, P.B. Shepson, J.W. Bottenheim, Geophys. Res. Lett. 28 (21) (2001) 4087–4090.
[23] S.P. Oncley, M. Buhr, D. Lenschow, D. Davis, S.R. Semmer, Atmos. Environ. 38 (32) (2004) 5389–5398.
[24] J.E. Dibb, L.G. Huey, D.L. Slusher, D. Tanner, Atmos. Environ. 38 (32) (2004) 5363–5500.
[25] L. Chu, C. Anastasio, J. Phys. Chem. A 107 (45) (2003) 9594–9602.
[26] T.L. Couch, A.L. Sumner, T.M. Dassau, P.B. Shepson, R.E. Honrath, Geophys. Res. Lett. 27 (15) (2000) 2241–2244.
[27] Y. Dubowski, A.J. Colussi, C. Boxe, M.R. Hoffmann, J. Phys. Chem. A 106 (30) (2002) 6967–6971.
[28] Y. Dubowski, M.R. Hoffmann, Geophys. Res. Lett. 27 (20) (2000) 3321–3324.
[29] Y. Dubowski, A.J. Colussi, M.R. Hoffmann, J. Phys. Chem. A 105 (20) (2001) 4928–4932.
[30] R.E. Honrath, S. Guo, M.C. Peterson, M.P. Dziobak, J.E. Dibb, M.A. Arsenault, J. Geophys. Res. Atmos. 105 (D19) (2000) 24183–24190.
[31] E.S.N. Cotter, A.E. Jones, E.W. Wolff, S.J.B. Bauguitte, J. Geophys. Res. Atmos. 108 (D4) (2003), art. no.-4147.
[32] J. Lee-Taylor, S. Madronich, J. Geophys. Res. Atmos. 107 (D24) (2002), art. no.-4796.
[33] E.W. Wolff, A.E. Jones, T.J. Martin, T.C. Grenfell, Geophys. Res. Lett. 29 (20) (2002), art. no.-1944.
[34] W.R. Simpson, M.D. King, H.J. Beine, R.E. Honrath, X.L. Zhou, Atmos. Environ. 36 (15–16) (2002) 2663–2670.
[35] F.N. Fisher, M.D. King, J. Lee-Taylor, J. Geophys. Res. Atmos., 2005JD005963RR, in press.
[36] L. Chu, C. Anastasio, J. Phys. Chem. A 109 (28) (2005) 6264–6271.
[37] H.W. Jacobi, R.C. Bales, R.E. Honrath, M.C. Peterson, J.E. Dibb, A.L. Swanson, M.R. Albert, Atmos. Environ. 38 (12) (2004) 1687–1697.
[38] T.M. Dassau, A.L. Sumner, S.L. Koeniger, P.B. Shepson, J. Yang, R.E. Honrath, N.J. Cullen, K. Steffen, H.W. Jacobi, M. Frey, R.C. Bales, J. Geophys. Res. Atmos. 107 (D19) (2002), art. no.-4394.
[39] A.M. Grannas, P.B. Shepson, T.R. Filley, Global Biogeochem. Cycles 18 (1) (2004), art. no.-GB1006.
[40] M.A. Granskog, H. Kaartokallio, Water Air Soil Pollut. 154 (1–4) (2004) 331–347.
[41] M.A. Hutterli, J.R. McConnell, R.C. Bales, R.W. Stewart, J. Geophys. Res. Atmos. 108 (D1) (2003), art. no.-4023.
[42] M.A. Hutterli, R. Rothlisberger, R.C. Bales, Geophys. Res. Lett. 26 (12) (1999) 1691–1694.
[43] P.B. Shepson, A.P. Sirju, J.F. Hopper, L.A. Barrie, V. Young, H. Niki, H. Dryfhout, J. Geophys. Res. Atmos. 101 (D15) (1996) 21081–21089.
[44] A.L. Sumner, P.B. Shepson, Nature 398 (6724) (1999) 230–233.
[45] M.A. Hutterli, J.R. McConnell, G. Chen, R. Bales, D. Davis, D. Lenschow, Atmos. Environ. 38 (32) (2004) 5423–5437.
[46] S. Houdier, S. Perrier, F. Domine, A. Cabanes, L. Legagneux, A.M. Grannas, C. Guimbaud, P.B. Shepson, H. Boudries, J.W. Bottenheim, Atmos. Environ. 36 (15–16) (2002) 2609–2618.
[47] J.E. Dibb, M. Arsenault, M.C. Peterson, R.E. Honrath, Atmos. Environ. 36 (15–16) (2002) 2501–2511.
[48] H. Boudries, J.W. Bottenheim, C. Guimbaud, A.M. Grannas, P.B. Shepson, S. Houdier, S. Perrier, F. Domine, Atmos. Environ. 36 (15–16) (2002) 2573–2583.
[49] J. Yang, R.E. Honrath, M.C. Peterson, J.E. Dibb, A.L. Sumner, P.B. Shepson, M. Frey, H.W. Jacobi, A. Swanson, N. Blake, Atmos. Environ. 36 (15–16) (2002) 2523–2534.
[50] A.M. Grannas, P.B. Shepson, C. Guimbaud, A.L. Sumner, M. Albert, W. Simpson, F. Domine, H. Boudries, J. Bottenheim, H.J. Beine, R. Honrath, X.L. Zhou, Atmos. Environ. 36 (15–16) (2002) 2733–2742.
[51] C. Guimbaud, A.M. Grannas, P.B. Shepson, J.D. Fuentes, H. Boudries, J.W. Bottenheim, F. Domine, S. Houdier, S. Perrier, T.B. Biesenthal, B.G. Splawn, Atmos. Environ. 36 (15–16) (2002) 2743–2752.
[52] P. Klan, J. Klanova, I. Holoubek, P. Cupr, Geophys. Res. Lett. 30 (6) (2003), art. no.-1313.
[53] J. Klanova, P. Klan, D. Heger, I. Holoubek, Photochem. Photobiol. Sci. 2 (10) (2003) 1023–1031.
[54] M.C. Peterson, R.E. Honrath, Geophys. Res. Lett. 28 (3) (2001) 511–514.
[55] D.K. Perovich, Ultraviolet radiation and the optical properties of sea ice and snow, in: D. Hessen (Ed.), UV Radiation and Arctic Ecosystems, Springer-Verlag, Berlin, Heidelberg, 2002.
[56] D.K. Perovich, US Army Corps of Engineers Cold Regions Research and Engineering Laboratory, vol. 33, 1996.
[57] B. Light, G.A. Maykut, T.C. Grenfell, J. Geophys. Res.-Oceans 108 (C2) (2003), art. no.-3051.
[58] D.K. Perovich, A.J. Gow, J. Geophys. Res.-Oceans 101 (C8) (1996) 18327–18343.
[59] R.A. Maffione, J.M. Voss, C.D. Mobley, Limnol. Oceanogr. 43 (1) (1998) 34–43.
[60] E.M. Haines, R.G. Buckley, H.J. Trodahl, J. Geophys. Res.-Oceans 102 (C1) (1997) 1141–1151.
[61] D. Miller, M.S. QuinbyHunt, A.J. Hunt, Appl. Opt. 36 (6) (1997) 1278–1288.
[62] H.J. Trodahl, R.G. Buckley, Science 245 (4914) (1989) 194–195.
[63] W.S. Pegau, J.R.V. Zaneveld, Cold Reg. Sci. Technol. 31 (1) (2000) 33–46.
[64] B. Light, G.A. Maykut, T.C. Grenfell, J. Geophys. Res.-Oceans 109 (C6) (2004), art. no.-C06013.
[65] M.D. King, W.R. Simpson, J. Geophys. Res.-Atmos. 106 (D12) (2001) 12499–12507.
[66] S.G. Warren, Rev. Geophys. 20 (1) (1982) 67–89.
[67] C.D. Mobley, G.F. Cota, T.C. Grenfell, R.A. Maffione, W.S. Pegau, D.K. Perovich, IEEE Trans. Geosci. Remote Sens. 36 (5) (1998) 1743–1749.
[68] D.K. Perovich, J. Geophys. Res.-Oceans 98 (C12) (1993) 22579–22587.
[69] B. Light, H. Eicken, G.A. Maykut, T.C. Grenfell, J. Geophys. Res.-Oceans 103 (C12) (1998) 27739–27752.
[70] S. Jiang, K. Stamnes, W. Li, B. Hamre, Appl. Opt. 44 (13) (2005) 2613–2625.
[71] K.I. Gjerstad, J.J. Stamnes, B. Hamre, J.K. Lotsberg, B.H. Yan, K. Stamnes, Appl. Opt. 42 (15) (2003) 2609–2622.
[72] J.D. Burley, H.S. Johnson, Geophys. Res. Lett. 19 (1992) 1359–1362.
[73] H.J. Trodahl, R.G. Buckley, Geophys. Res. Lett. 17 (1990) 2177–2179.
[74] G. Wendler, T. Quakenbush, Antarctic J. (1993) 84–85.
[75] D.K. Perovich, Geophys. Res. Lett. 22 (1995) 1349–1352.

[76] D.K. Perovich, C.S. Roesler, W.S. Pegau, J. Geophys. Res.-Oceans 103 (C1) (1998) 1193–1208.
[77] D.K. Perovich, D.G. Barber, G.F. Cota, A.J. Gow, T.C. Grenfell, J. Longacre, R.A. Maffione, C.D. Mobley, R.G. Onstott, W.S. Pegau, C.S. Roesler, IEEE Trans. Geosci. Remote Sens. 36 (1998) 1633–1641.
[78] T.C. Grenfell, G.A. Maykut, J. Glaciol. 18 (1977) 455–463.
[79] D.N. Thomas, S. Papadimitriou, Biogeochemisty of sea ice, in: D.N. Thomas, G.S. Dieckmann (Eds.), Sea Ice: An Introduction to its Physics, Chemistry, Biology and Geology, Blackwell publishing, Oxford, 2003, pp. 267–302.
[80] H. Kennedy, D.N. Thomas, G. Kattner, C. Haas, G.S. Dieckmann, Mar. Ecol.—Prog. Ser. 238 (2002) 1–13.
[81] A. Sigg, T. Staffelbach, A. Neftel, J. Atmos. Chem. 14 (1–4) (1992) 223–232.
[82] R. Weller, O. Schrems, Geophys. Res. Lett. 20 (2) (1993) 125–128.